Physics of Fluids

# Flow dynamics and azimuthal behavior of the self-excited acoustic modes in axisymmetric shallow cavities

Cite as: Phys. Fluids **32**, 115109 (2020); https://doi.org/10.1063/5.0026552
Submitted: 25 August 2020 . Accepted: 12 October 2020 . Published Online: 04 November 2020

Moamenbellah Abdelmwgoud, Mahmoud Shaaban, and Atef Mohany

View Online Export Citation CrossMark

ARTICLES YOU MAY BE INTERESTED IN

On the three-dimensional flow development around circular finned cylinders
Physics of Fluids **32**, 115116 (2020); https://doi.org/10.1063/5.0026603

Spinning behavior of flow-acoustic resonant fields inside a cavity: Vortex-shedding modes and diametral acoustic modes
Physics of Fluids **32**, 085109 (2020); https://doi.org/10.1063/5.0019112

Vortex dynamics and acoustic sources in the wake of finned cylinders during resonance excitation
Physics of Fluids **32**, 075117 (2020); https://doi.org/10.1063/5.0016076




AIP Publishing



© 2020 Author(s).

Physics of Fluids ARTICLE scitation.org/journal/phf

# Flow dynamics and azimuthal behavior of the self-excited acoustic modes in axisymmetric shallow cavities

Cite as: Phys. Fluids 32, 115109 (2020); doi: 10.1063/5.0026552
Submitted: 25 August 2020 • Accepted: 12 October 2020 •
Published Online: 4 November 2020

View Online Export Citation CrossMark

Moamenbellah Abdelmwgoud, Mahmoud Shaaban, and Atef Mohany[a)]

## AFFILIATIONS

Aeroacoustics and Noise Control Laboratory, University of Ontario Institute of Technology, 2000 Simcoe Street North, Oshawa, Ontario L1G 0C5, Canada

[a)]Author to whom correspondence should be addressed: atef.mohany@ontariotechu.ca

## ABSTRACT

Self-excitation of acoustic resonance in axisymmetric cavities can lead to a complex flow–acoustic coupling, which may result in severe noise generation. In this work, a large eddy simulation is performed to model the different flow–sound coupling mechanisms during the self-excitation of various excitable acoustic modes in an axisymmetric shallow cavity configuration with an aspect ratio of L/d = 1 over the lock-in region. The compressible Navier–Stokes equations are solved at a resolution sufficient to capture the flow and the acoustic dynamics. The excitation of three acoustic modes of different aerodynamic characteristics over the range of the tested flow velocities was observed. These modes are a stationary diametral mode, a spinning diametral mode, and a longitudinal mode. The initiation and separation of vortices over the cavity mouth accompanying the self-excitation of each mode involve different dynamics. If two antisymmetric series of vortical crescents separate successively at the leading edge, a stationary acoustic mode is excited. The formation of a continuously rotating helical vortex, connecting the leading edge and the trailing edge, leads to the excitation of the diametral spinning mode. The excitation of the longitudinal mode is associated with symmetric rings of vortices. Complex patterns of flow velocities and Reynolds stresses in the circumferential direction are observed for the diametral modes but not for the longitudinal mode. In all cases, the excitation of acoustic resonance requires a synchronization of the vortex separation and impingement processes, which is necessary for efficient feedback to sustain the flow–sound coupling mechanism.

*Published under license by AIP Publishing.* https://doi.org/10.1063/5.0026552

## NOMENCLATURE

| | |
|---|---|
| $D$ | cavity diameter |
| $d$ | cavity depth |
| $D_p$ | pipe diameter |
| $f_a$ | acoustic mode frequency |
| $f_v$ | shear layer mode frequency |
| $L$ | cavity length |
| $p$ | instantaneous acoustic pressure |
| $P^*$ | normalized acoustic pressure |
| $P_{rms}$ | root mean square acoustic pressure |
| $St_v$ | Strouhal number |
| $U_\infty$ | free stream velocity |
| $u_R$ | radial velocity component |
| $U_r$ | reduced flow velocity |
| $u_x$ | stream wise velocity component |
| $u_\theta$ | tangential velocity component |
| $y$ | distance from the pipe wall in the radial direction |
| $\theta$ | azimuthal angle |
| $\phi$ | temporal phase angle |
| $\omega$ | vorticity |

## I. INTRODUCTION

The excitation of acoustic resonance by an internal flow is a design concern in many engineering applications. Under certain conditions, periodic flow instabilities can couple with the natural acoustic modes of the flow-conveying duct, leading to incidents of acoustic resonance excitation. The resulting strong acoustic oscillations have been reported in heat exchangers and boilers,[1,2] cylinders,[3–6] pipes,[7–9] side branches,[10,11] combustion chambers,[12,13] gate


Published under license by AIP Publishing

valves,[14] and turbomachines.[15,16] The excited acoustic resonance starts abruptly and is often associated with acute noise and intense vibration and can lead to fatigue and damage of equipment.[17] Recent experimental evidence showed that flow periodicities are capable of exciting the diametral acoustic modes in coaxial configurations, such as annular combustors,[12,18] propulsion engines,[19] and piping systems.[20,21] In these cases, the interaction of the flow and acoustic fields occurs in the streamwise and transverse directions, leading to an intricate pattern of flow and acoustic phenomena. Although the mechanism that leads to excitation of acoustic resonance is relatively well understood for the case of rectangular cavities, the effect of the circular symmetry of the coaxial configuration on the flow–acoustic coupling is not yet fully understood. Under normal conditions, the flow separation over cavities results in negligible production of acoustic power due to the periodic flapping of the shear layer over the mouth of the cavity.[22] Under certain conditions, however, extreme acoustic oscillations can be excited due to a fluid-resonant mechanism.[23] Rossiter[24] reported that vortices separating at the leading edge of cavities are convicted downstream to impinge on the trailing edge, releasing pressure oscillations with a frequency that depends on the flow velocity and the cavity length. If the frequency of the pressure oscillations coincides with the frequency of an acoustic mode of the duct, the flow and the acoustic field can become coupled, organizing and strengthening the separation and impingement, leading to the excitation of severe acoustic resonance.[25,26] This feedback results in the coupling of the acoustic mode with the periodic separation and impingement of vortices, leading to a lock-in of their frequencies and a significant increase in the acoustic pressure. Most of the available literature report investigations of the acoustic response of rectangular cavities, leading to the excitation of either transverse[27,28] or longitudinal modes,[29,30] using experimental[31] and numerical[32] techniques. On the other hand, the excitation of the acoustic diametral modes of axisymmetric cavities has only been under investigation recently. Analytic evidence of the existence of excitable diametral modes in infinite cylindrical waveguides was first provided by Evans, Levitin, and Vassiliev.[33] The susceptibility of acoustic modes to excitation by flow instability depends on the geometry of flow boundaries, as well as the orientation of the acoustic mode with respect to the flow perturbation.

An axisymmetric cavity is formed by the symmetric rotation of a two-dimensional cavity configuration around the streamwise symmetry axis. In the absence of the mean flow, Hein, Koch, and Nannen[34] numerically showed that the axisymmetric geometry could create perfectly acoustic trapped modes that have antisymmetric pressure oscillations and no preferred azimuthal orientation. In such a case, the excited acoustic modes have a frequency that is lower than the cutoff frequency of the duct. Keller and Escudier[35] experimentally investigated the excitation of the diametral modes of an annular cavity connected to a pipe through a thin annular opening. Although the observed acoustic mode was stationary, its azimuthal orientation changed as each experimental configuration was assembled, suggesting that it takes a preferred position due to deviations from a perfect axisymmetric configuration. Awny and Ziada[36] experimentally investigated the flow-excited resonances of the acoustic diametral modes of a cylindrical pipe housing an axisymmetric shallow cavity, observing intense acoustic pressure levels reaching up to 170 dB associated with lock-in over a wide range of flow velocities. In a series of experimental investigations, Aly and Ziada[21,37–39] provided a description of the aeroacoustic characteristics of axisymmetric shallow cavities, providing extensive details of the effect of the cavity geometry on the acoustic resonance level and acoustic pressure patterns. Results indicated that diametral acoustic modes, with their acoustic pressure nodes at the axis and pressure antinodes at the circumference of the cavity floor, can be excited by the flow in the duct. Because these modes have no preferred location for the pressure antinode along the outer circumference, they can spin around the duct streamwise symmetry axis. As a result, the excited modes are stationary at low flow velocities, but they switch to spinning mode pattern at higher velocities. Notably, small geometrical deviations from axisymmetry and localized damping effects introduce an orientation preference that results in partially spinning behavior. The acoustic characteristics of the first excited acoustic mode are significantly influenced by the mean flow velocity. Their results also showed that the acoustic pressure at resonance increases as the cavity becomes shorter or deeper relative to the main pipe diameter. Moreover, the cavity length to depth ratio controls the amplitudes of the various excited diametral and longitudinal modes. However, this set of investigations did not include any aspects of the flow field or the influence of diametral or longitudinal mode excitation on the structure of the separated shear layer on the cavity mouth and did not provide details of the flow dynamics that take place as modes of different azimuthal behaviors are excited. Oshkai and Barannyk[40] experimentally measured the acoustic pressure at different azimuthal locations on the wall of an axisymmetric cavity, confirming that the geometries of the leading and trailing edges of the cavity have an effect on the acoustic pressure amplitude. They also indicated that spinning modes are excited after a threshold of Mach number is exceeded, whereas stationary or partially spinning modes can be observed at lower flow velocities. Thirumoorthy, Chakravarthy, and Brahmanandam[41] experimentally investigated the excitation of the acoustic diametral modes using a pressure transducer, showing that the streamwise shape of the cavity has a significant effect on the resonance pressure amplitude.

Compared with the significant efforts carried out to identify the acoustic characteristics of the diametral mode excitation in axisymmetric cavities, very limited reports of the dynamics of the flow field during resonance excitation are available in the literature. Oshkai and Barannyk[42] used particle image velocimetry to visualize the instantaneous vorticity field of the first shear layer mode during excitation of the diametral acoustic modes. Ziada, Bolduc, and Lafon[43] investigated the excitation of diametral modes within a rectangular cavity attached to a circular pipe. Due to the preferential azimuthal orientation of the square cavity, complex stationary and spinning mode patterns were observed. The interaction of two orthogonal modes was shown to generate spinning behavior that is associated with a helical vortex structure between the cavity leading and trailing edges. More recently, Wang and Liu[44] carried out a three-dimensional (3D) zonal large eddy simulation (LES) of the flow dynamics of an axisymmetric cavity under conditions that give rise to the maximum resonance intensity. The numerical model was able to capture the acoustic frequencies and the spinning helical structure of the first three diametral acoustic modes. Results showed that the flow field, when coupled with the spinning modes at their maximum intensity, possesses a complex 3D vortex structure.


Published under license by AIP Publishing

Wang and Liu[45] suggested that two separate vortex shedding modes are responsible for the spinning motion. However, Wang and Liu[44,45] only studied pure spinning modes at a single cavity configuration and did not present aspects of the flow dynamics during excitation of longitudinal or diametral modes of different azimuthal behaviors. On the other hand, Shaaban and Ziada[46] carried out particle image velocimetry measurements on a rectangular cavity in a pipe during excitation of the pipe longitudinal modes, showing that the strong acoustic oscillations synchronize and strengthen vortex shedding at the leading edge, creating a sound source over the cavity mouth. Results showed a pronounced effect of the strong acoustic oscillations on the flow dynamics. Yet, Shaaban and Ziada[46] did not consider a circular cavity configuration and did not observe the excitation of diametral modes. As a result, the nature of the coupling associated with the excitation of modes that have different azimuthal behaviors in an axisymmetric cavity has not been clarified.

From the foregoing discussion, it becomes clear that the effect of flow–acoustic coupling on the flow dynamics of axisymmetric cavities is not yet well understood. The different azimuthal behaviors of the excited diametral and longitudinal acoustic modes at different flow velocities are bound to have a significant effect on the flow dynamics at the cavity mouth, which had not been previously identified. Moreover, the modal characteristics of the acoustic pressure and the flow fluctuations over the cavity need to be investigated. In addition, investigating the behavior of the coupled acoustic–flow fields over the lock-in region can help identify the critical changes in the flow separation, impingement over an acoustic cycle, its role in initiating specific acoustic modes, and determining their azimuthal behaviors. Understanding the details of this mechanism is particularly critical to enable finding ways to mitigate resonance excitation and control its potentially destructive oscillations. Therefore, this work presents a numerical study of the flow dynamics and the azimuthal behaviors of the flow-excited acoustic modes of axisymmetric cavities using large eddy simulations. The coupled flow–acoustic field is directly simulated for a range of flow velocities that result in the self-excitation of stationary, spinning, and longitudinal acoustic modes by the flow over an axisymmetric cavity of a length to depth ratio of 1.0. The aeroacoustic response of the axisymmetric cavity, including the phase characteristics of the acoustic pressure at the cavity walls, is numerically identified. Results of the acoustic pressure and flow characteristics' development at different flow velocities are used to elucidate the effect of the azimuthal behavior of the excited mode on the flow dynamics to help identify efficient control strategies.

## II. METHODOLOGY

In this study, the coupling between the air flow and acoustic fields over an axisymmetric cavity is studied by means of three-dimensional Large Eddy Simulations (LESs). A schematic of the computational domain and the used mesh are shown in Fig. 1. The domain of interest consists of a cylindrical cavity of an outer diameter $D$ = 200 mm, a length $L$ = 25 mm, and a depth $d$ = 25 mm, forming a cavity with an aspect ratio of $L/d = 1$. The cavity is axisymmetrically attached to a pipe with a diameter $D_p$ = 150 mm. The pipe extends 3 diameters ($3D$) in the upstream and downstream

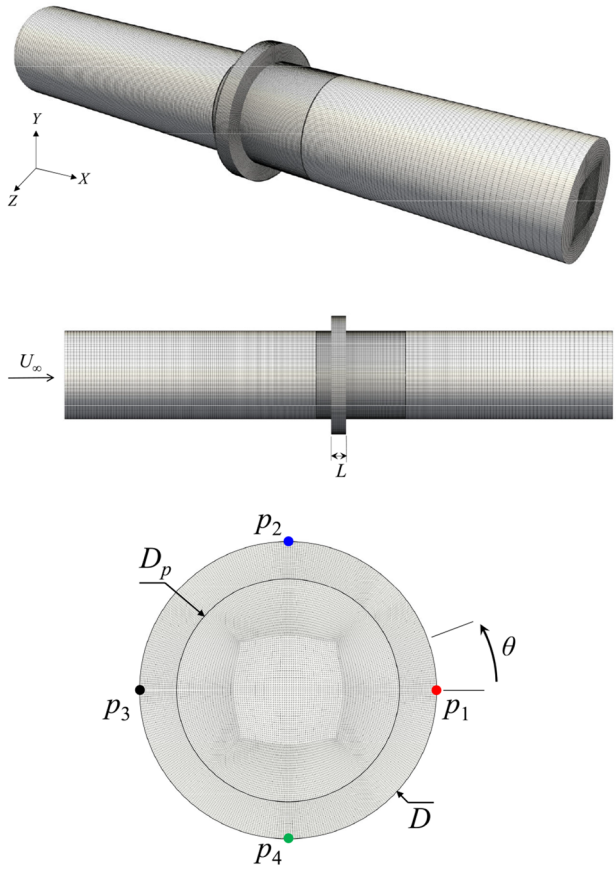



**FIG. 1**. Flow domain, mesh details, and pressure monitors' location.

directions in order to enable flow development and prevent any significant effect of the inlet and exit boundary conditions on the cavity region and reduce the effect of acoustic radiation from the test section ends.[47] These dimensions were based upon the experimental investigation of Aly and Ziada[38] to provide a base for validation of the results.

A fully coupled transient solver for compressible turbulent flows was deployed on the open source OpenFOAM computational fluid dynamics library to solve the transient three-dimensional Navier–Stokes equations in order to obtain the flow dynamics and the aeroacoustic response. The PIMPLE algorithm, which is a combination of the PISO and the SIMPLE algorithms, was used to resolve the pressure–velocity coupling by solving the governing equations of continuity, momentum, and energy balance for Newtonian fluids.[48] The thermophyiscal properties of air including molecular viscosity, Prandtl number, and specific heat at constant volume are used at their values at 20 °C. The density and internal energy are modeled according to the ideal gas equation of state. The Smagorinsky model was used to model the turbulence in the subgrid scale by solving the subgrid-scale kinetic energy $k_{sgs}$ equation, as it provides accurate predictions in axisymmetric flows, as shown by Lee and Cant.[49] The large eddy stress tensor is associated with the


Published under license by AIP Publishing

subgrid-scale stress tensor through the subgrid-scale viscosity, represented as follows:

$$\tau_{ij} \approx \frac{2}{3}k_{sgs}\delta_{ij} - 2\nu_{sgs}(\overline{D}^{*})_{ij}, \quad (1)$$

where $\tau_{ij}$ is the subgrid-scale stress tensor, $\nu_{sgs}$ is the subgrid-scale viscosity, and $k_{sgs}$ is the subgrid-scale kinetic energy. The asterisk denotes the deviatoric components of the large-scale strain rate tensor.

The subgrid-scale kinetic energy is calculated as

$$k_{sgs} = \frac{1}{2}\tau_{kk} = \frac{1}{2}(\overline{u_k u_k} - \overline{u}_k\overline{u}_k). \quad (2)$$

The subgrid-scale viscosity is related to the kinetic energy as

$$\nu_{sgs} = C_k\sqrt{k_{sgs}}\Delta, \quad (3)$$

where $C_k$ is a model constant, with a value of 0.094. The subgrid-scale kinetic energy production, dissipation, and diffusion are accounted by solving a transport equation, as theoretically derived by Yoshizawa and Horiuti.[50] The grid size $\Delta$ that defines the subgrid length scale is calculated using a van Driest damping function in the near-wall region. The spectral characteristics of the flow velocity show a good agreement with the predicted turbulence energy cascade over the frequency range of interest. The second-order implicit backward Euler scheme was used for temporal discretization. A Gauss linear-upwind scheme is used for the spatial discretization of the convective terms in the momentum equation, and a Gauss linear gradient differentiation scheme is used for the diffusive terms. All the implemented schemes had second-order accuracy to enable self-initiation and fine resolution of the transient and periodic flow structures.[51]

The simulation is performed at nine inlet flow velocities from $U_\infty$ = 50 m/s to 75 m/s, corresponding to a Reynolds number range between $8.2 \times 10^4$ and $1.2 \times 10^5$ based on the cavity length $L$. Over this range, previous experiments by Aly and Ziada[39] suggested a change in the azimuthal behavior of the excited acoustic mode. As will be discussed in details hereafter, the flow velocity determines whether the excited mode is stationary or spinning, which enables the investigation of the differences to the mechanism of excitation.

The flow domain, shown in Fig. 1, is meshed into a hexahedron structured grid with $8 \times 10^5$ elements in the inlet and outlet pipes, and $1.5 \times 10^6$ nodes in the cavity section. The element size is set to insure a convective Courant number of less than 0.8 and an acoustic Courant number of less than 4.0 all over the flow domain. The inlet boundary condition is set as a velocity inlet with uniform velocity $U_\infty$. An outflow boundary is specified at the outlet. The pressure on the inlet and outlet boundaries is modeled using a non-reflecting wave-transmissive condition. A wall function is used to model the flow in the near-wall region according to the logarithmic law of the wall with a stepwise implementation.[52] The value of $y^+$ at the leading and trailing edges ranges from 28 to 37, allowing for accurate application of the wall function.[53] Pressure monitor points are located on the wall of the cavity to capture the amplitude and phase characteristics of the excited resonance in a form comparable to available experimental studies. The azimuthal angle $\theta$ is counterclockwise with the location of the pressure monitor $p_1$ as a reference following a right hand rule with the coordinate system, as shown in Fig. 1.

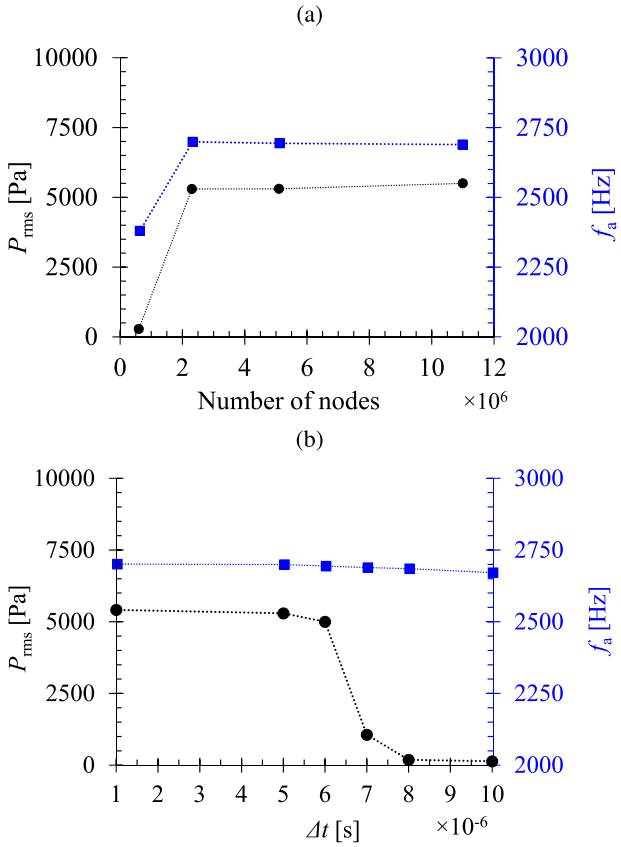



**FIG. 2**. Effect of (a) the number of mesh nodes and (b) the time step on the predicted acoustic pressure amplitude and dominant frequency at an inlet flow velocity of $U_\infty$ = 64 m/s.

A sensitivity analysis was carried out to ensure that the results have no dependency on the time step or the mesh node count. The data in Fig. 2 show the acoustic pressure and dominant frequency on the cavity wall at an inlet flow velocity of $U_\infty$ = 64 m/s for different meshes and time steps. The tested meshes were created by splitting elements in the dense cavity zone. The time step and the number of elements did not show any significant effect on the frequency of the oscillations, as the instability can be predicted using a lower temporal and spatial resolution than necessary to resolve the flow–acoustic coupling.[54] Using a time step higher than $6 \times 10^{-6}$ s results in a decrease in the predicted acoustic pressure amplitude. At a time step of $8 \times 10^{-6}$ s, the instability is still captured as a dominant frequency, but the amplitude drops down near background noise levels, signaling that the acoustic Courant number is larger than necessary to resolve the flow–acoustic coupling and predict self-excitation of resonance.

Figure 3 shows the normalized predicted acoustic pressure, defined using the reference density $\rho_0$ of air at 20 °C as follows:

$$P^* = \frac{2P_{rms}}{\rho_0 U_\infty^2}. \quad (4)$$


Published under license by AIP Publishing

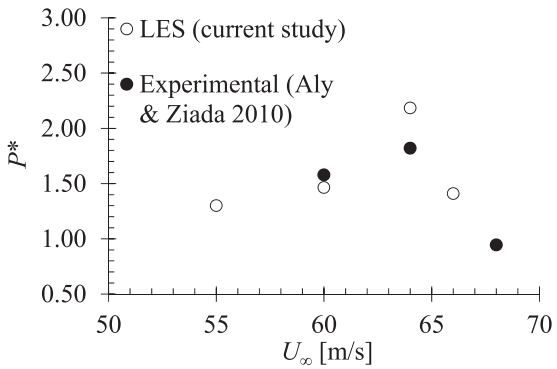



**FIG. 3**. Computational model prediction of the normalized aeroacoustic pressure over the lock-in range compared with the observations of Aly and Ziada.[38] Reproduced with permission from K. Aly and S. Ziada, "Flow-excited resonance of trapped modes of ducted shallow cavities," J. Fluids Struct. **26**(1), 92–120 (2010). Copyright 2010 Elsevier.

Figure 3 shows a good agreement between the predicted aeroacoustic response and that observed experimentally by Aly and Ziada[38] for a cavity with the same dimensions. The peak normalized pressure is captured at the same upstream flow velocity of $U_\infty = 64$ m/s. A further increase in flow velocity results in a decrease in the normalized acoustic pressure. In addition, Fig. 4 shows the flow velocity profile temporally averaged at a flow velocity of 31 m/s at the upstream edge of the cavity, compared with the hotwire results of Aly and Ziada[38] at the same location, flow velocity, and cavity dimensions. The velocity profile confirms that the flow is fully developed prior to separation. A clear agreement between the current model predictions and the experimental results asserts the accuracy of the simulation in capturing details of the flow separation. The boundary profile and momentum thickness at the leading edge, which are vital parameters that determine the flow dynamics over the cavity mouth, are accurately predicted.

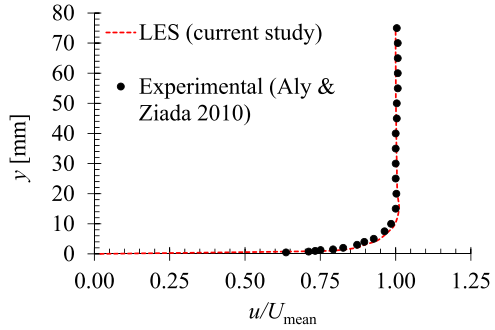



**FIG. 4**. Comparison of the average radial boundary layer profile at the cavity leading edge over a cycle of vortex shedding in comparison with experimental hotwire measurements of Aly and Ziada.[38] Reproduced with permission from K. Aly and S. Ziada, "Flow-excited resonance of trapped modes of ducted shallow cavities," J. Fluids Struct. **26**(1), 92–120 (2010). Copyright 2010 Elsevier.

## III. AEROACOUSTIC RESPONSE OF AN AXISYMMETRIC CAVITY

In this section, the results of the large eddy simulation of the coupled flow–sound fields over a range of flow velocities are discussed to illustrate the flow dynamics that lead to different acoustic pressure and azimuthal characteristics of the excited acoustic modes. Figure 5 shows the normalized acoustic pressure $P^*$ as defined in Eq. (4) for a range of reduced velocities $U_r$,

$$U_r = \frac{U_\infty}{f_a L}, \tag{5}$$

where $f_a$ is the acoustic mode frequency and $L$ is the characteristic length, set as the cavity length between the leading and trailing edges. The computational model is able to predict a typical lock-in behavior, similar to that observed in experimental studies of axisymmetric cavities.[21] An increase in the reduced velocity from $U_r = 0.8$ to 0.93 triggered a clear increase in the normalized pressure $P^*$ from 1.3 to 2.2. A further increase beyond $U_r = 0.93$ resulted in a drop of $P^*$ to its previous levels. A further increase in the reduced velocity up to $U_r = 1.28$ results in a gradual increase in the value of $P^*$ to 1.8. Such behavior indicates that an excitation source is present and is related to the second shear layer mode, which occurs at a Strouhal number $St_v$ close to 1.0, defined as follows:

$$St_v = \frac{f_v L}{U_\infty} = \frac{n - \alpha}{M + \frac{1}{\kappa}}, \tag{6}$$

where $f_v$ is the $n$th shear layer mode frequency and $\kappa$ and $\alpha$ are empirical constants that correspond to the average convection speed of the vortices in the shear layer and a phase delay, respectively. For turbulent flows, the value of $1/\kappa$ is typically 1.75 and $\alpha$ is typically equal to 0.25.[24] Figure 5 shows that the increase in flow velocity leads to the excitation of acoustic modes of three different azimuthal mode behaviors. The three modes are distinguishable by the pattern of the acoustic pressure in the cavity cross section as well as whether the pattern spins around the cavity axis, as will be discussed in the following sections. Notably, the three excited modes are all variant across the cavity cross section only so that the acoustic pressure distribution is uniform over the length of the cavity. Modes of higher orders in the streamwise direction are expected to have much higher frequencies than modes excited in this study due to the low cavity length to diameter ratio $L/d$. At the lowest range of reduced

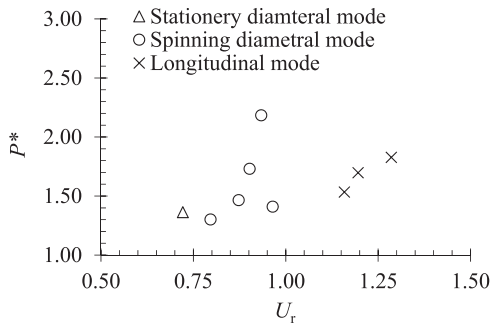



**FIG. 5**. The effect of the reduced velocity on the normalized pressure and the azimuthal behavior of the excited mode for an axisymmetric cavity of a length to depth ratio of $L/d = 1$.


Published under license by AIP Publishing

velocities, up to $U_r = 0.75$, a stationary diametral mode is observed. Between reduced velocities of $U_r = 0.75$ and 1.00, the excited mode spins. Increasing the reduced flow velocity $U_r$ beyond 1.00 results in the excitation of a longitudinal acoustic mode. The following discussion illustrates the characteristics of each of the three different modes and elucidates the coupled flow–acoustic dynamics that lead to the excitation of each azimuthal behavior.

## IV. AZIMUTHAL BEHAVIOUR OF EXCITED ACOUSTIC MODES

The pressure characteristics of the three different excited acoustic modes can be illustrated by inspecting the pressure contours at the middle cross section of the cavity over a complete acoustic cycle during lock-in, as shown in Fig. 6 (multimedia view). At $U_\infty = 50$ m/s, a stationary diametral mode is observed. The acoustic frequency of this mode is $f_a = 2728$ Hz. The acoustic pressure at four equally spaced instants on the acoustic cycle is shown in Fig. 6(a) (multimedia view), depicted by the temporal phase angle $\phi$, referred to the start of the acoustic cycle $\phi = 0$. This mode is characterized by stationary oscillations of the acoustic pressure that are antisymmetric over two opposite sides of the cross section of the cavity. Two nodal acoustic pressure planes extend in the streamwise $x$ direction. The first nodal plane intersects with the cross section at a straight line that has an azimuthal angle of $\theta \approx 90°$. The second nodal plane intersects with the cross section at a circle that coincides with the

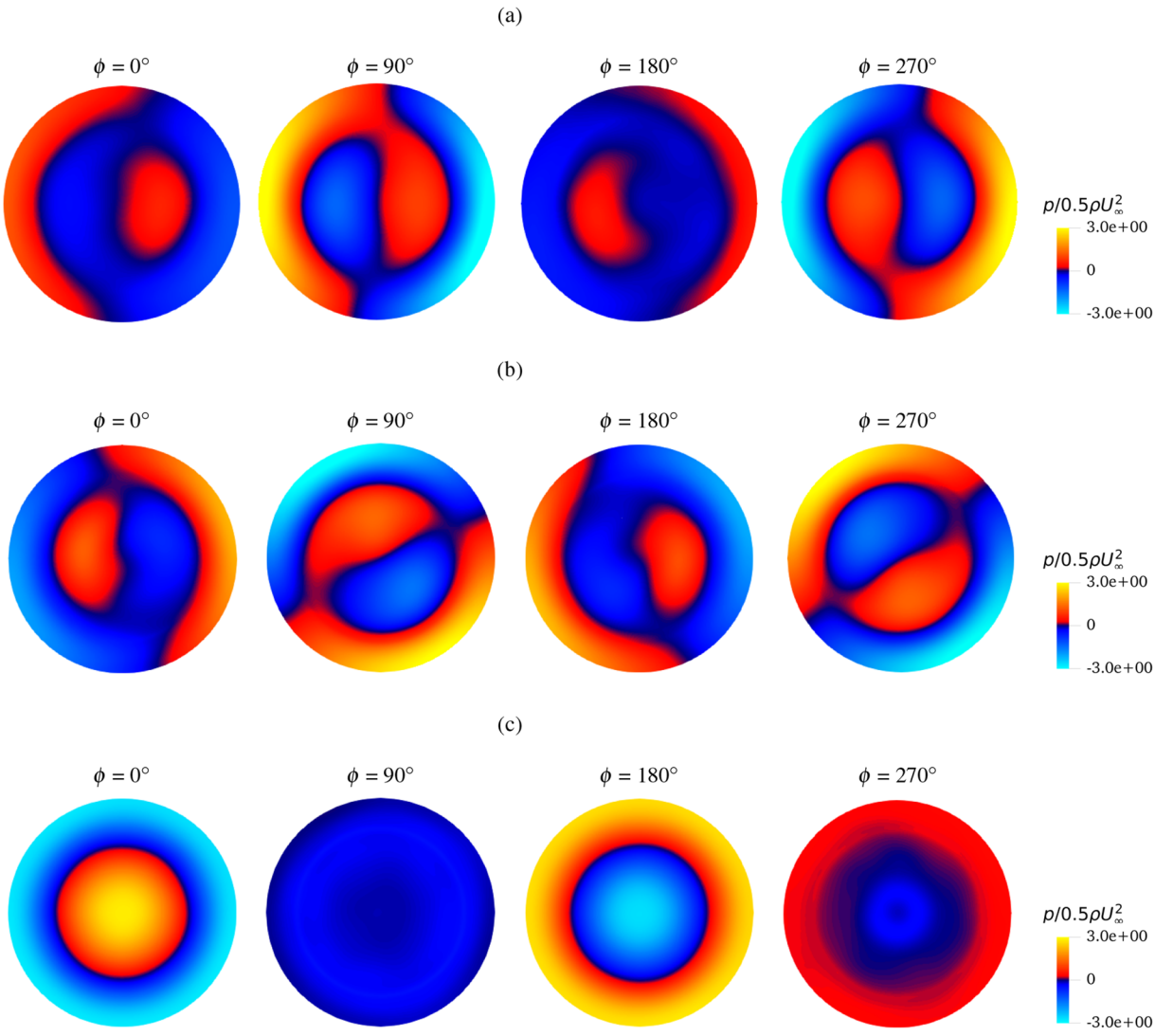



**FIG. 6**. The instantaneous pressure normalized by the maximum dynamic pressure in the middle cross section of the cavity at four equally spaced instants of the acoustic cycle at three different flow velocities. (a) Stationary acoustic diametral mode, $U_\infty = 50$ m/s, (b) spinning acoustic diametral mode, $U_\infty = 64$ m/s, and (c) longitudinal mode, $U_\infty = 75$ m/s. Multimedia view: (a) https://doi.org/10.1063/5.0026552.1; (b) https://doi.org/10.1063/5.0026552.2; and (c) https://doi.org/10.1063/5.0026552.3


Published under license by AIP Publishing

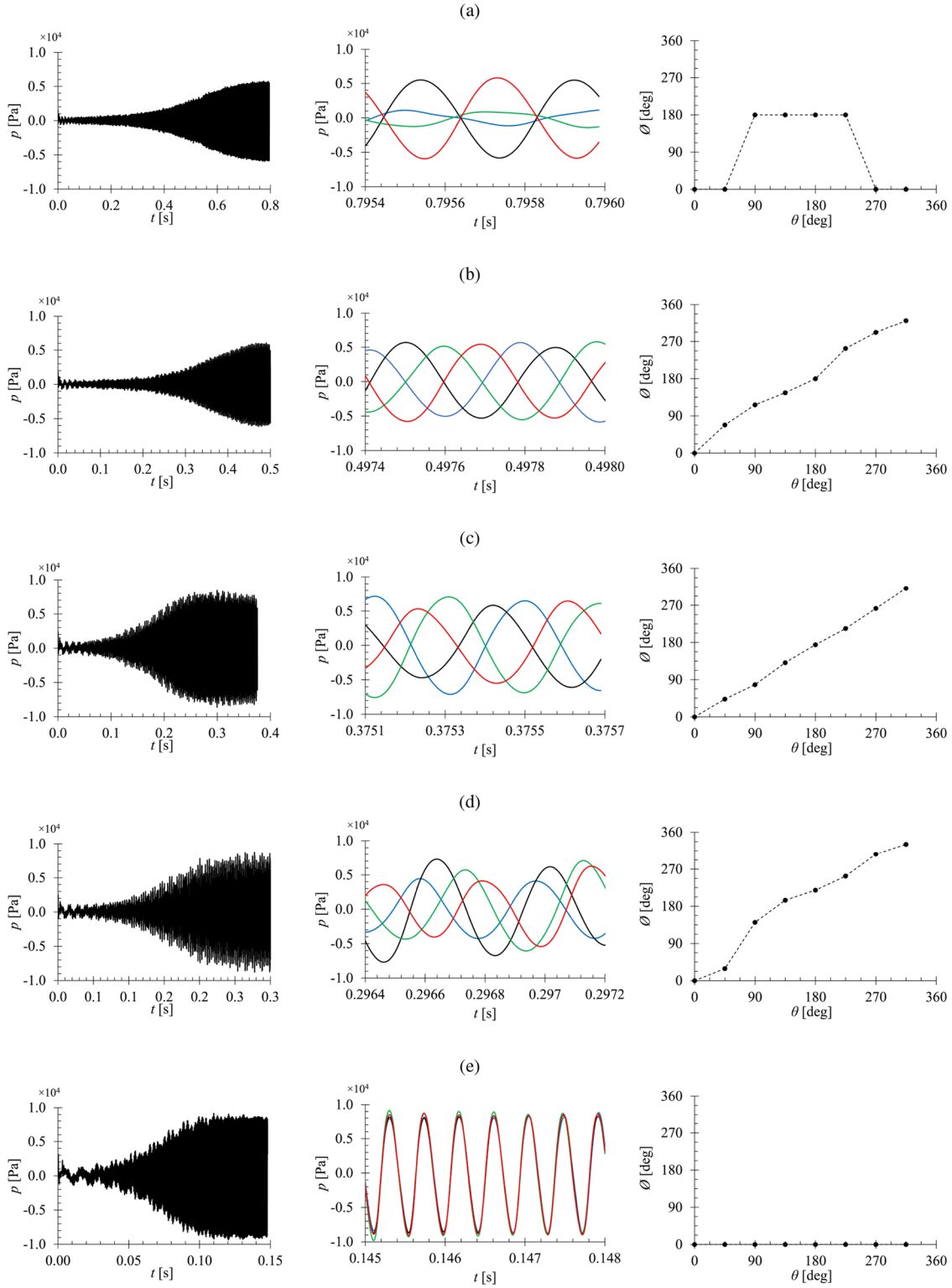



**FIG. 7**. The progress of acoustic pressure over the outer wall of the cavity at different flow velocities. (a) Stationary acoustic diametral mode, $U_\infty$ = 50 m/s, (b) partially spinning diametral mode, $U_\infty$ = 55 m/s, (c) spinning diametral mode, $U_\infty$ = 64 m/s, (d) partially spinning diametral mode, $U_\infty$ = 66 m/s, and (e) longitudinal mode, $U_\infty$ = 75 m/s.


Published under license by AIP Publishing

circumference of the pipe wall. On the two sides of the straight nodal plane, the pressure has a second-order diametral distribution with two stationary antinodes that are antisymmetric with each other on the two sides of the circular nodal plane. The two halves of the cross section are antisymmetric with each other. The whole distribution is stationary in the azimuthal direction $\theta$ such that the nodal planes keep their positions over the cycle.

As the flow velocity increases to $U_\infty = 64$ m/s, a spinning mode is observed. In this case, Fig. 6(b) (multimedia view) shows spatially similar pressure distribution over the cross section. The frequency of this mode is $f_a = 2699$ Hz. Over the span of the acoustic cycle, however, a completely different variation of the acoustic pressure distribution takes place. While the cylindrical nodal plane is stable, the straight nodal plane rotates around the streamwise axis of the cross section. The two halves of the cross section stay opposite and antisymmetric with each other, keeping nearly stable values of acoustic pressure over time while rotating one complete circle over the lock-in frequency acoustic cycle. Two antinodes with the highest and lowest values of acoustic pressure rotate along the cavity outer wall, antisymmetric with two other antinodes that have generally lower acoustic pressure values. This spinning behavior occurs in a streamwise direction. The direction of spinning is theoretically arbitrary, and therefore, the result obtained in the simulation is subject to the computational conditions.

As the flow velocity increases to $U_\infty = 75$ m/s, a longitudinal mode is excited. This mode has nodal and antinodal planes in the streamwise $x$ direction and also has a second-order distribution in the cross section of the cavity. No straight nodal planes split the cross section. Over the complete acoustic cycle, the pressure contours in Fig. 6(c) (multimedia view) show that the acoustic pressure over the outer wall of the cavity has a fixed phase, with the same instantaneous value over the whole circumference. The pressure changes from a maximum to a minimum over the outer wall in the same time. On the other side of the cylindrical nodal plane, closer to the center line of the pipe, the pressure is antisymmetric with the pressure on the outer wall, with generally lower acoustic pressure.

To further investigate the progress of acoustic resonance excitation for the different modes as the flow velocity changes over the range of lock-in, Fig. 7 shows the temporal and spatial development of the acoustic pressure on the wall of the cavity at different upstream flow velocities. The first column shows the development of the acoustic pressure signal detected at the monitor location $p_1$ for five different flow velocities until the acoustic pressure stabilizes into statistically stable oscillations of a steady amplitude. Notably, the simulated time required for the case to reach a steady oscillation amplitude decreases significantly as the flow velocity increases, such as 0.8 s is required at $U_\infty = 50$ m/s and only 0.1 s is required at $U_\infty = 75$ m/s. Careful inspection suggests that this value depends on the square of the upstream flow velocity $U_\infty^2$, indicating a dependency on the flow kinetic energy, in agreement with experimental evidence for other acoustic resonance excitation mechanisms.[55] This can reasonably be expected, as flows can excite and sustain a stronger acoustic resonance in proportion with the available kinetic energy.

In the middle column of Fig. 7, we take a closer look at the development of the acoustic pressure on the wall of the cavity over a small number of acoustic cycles at different upstream flow velocities for steady-state oscillations. In the five figures, the colors of the lines are consistent with the location of the four pressure monitors shown in Fig. 1. At $U_\infty = 50$ m/s, a stationary mode is excited. The acoustic pressure on the outer wall shows a pattern of differences in phase and amplitude such that peaks and troughs coincide with each other. All microphones pass through the value of $p = 0$ at the same instant. As the flow velocity increases to $U_\infty = 55$ m/s, the mode starts to have a spinning component, the acoustic pressure amplitudes at the four monitors become closer to each other, and start to have their peaks at different instants of the cycle. A further increase in acoustic pressure values is observed at $U_\infty = 64$ m/s, where the peak acoustic pressure is observed. A further increase in flow velocity to $U_\infty = 66$ m/s results in a drop in the amplitudes of acoustic pressure, a variation in the amplitudes, and a change in the phase differences between the peaks as the mode starts to exit its pure spinning behavior. At $U_\infty = 75$ m/s, the excited mode is longitudinal, and the acoustic pressure amplitudes at the four monitors, and in fact along the whole circumference, have the same value and the same phase over the whole acoustic cycle.

The right column of Fig. 7 shows the phase of the acoustic pressure signal at eight equally spaced locations over the circumference of the cavity middle cross section at different upstream flow velocities. All phase angles $\phi$ are referred to the pressure signal at the location of the monitor $p_1$ for comparison. At $U_\infty = 50$ m/s, the stationary behavior is evident by the pattern of clear phases in the figure. Four of the monitors sustain a phase of $\phi = 0°$, while the other four have a consistent phase of $\phi = 180°$. The two groups are separated by the nodal line azimuthal angle, close to $\theta = 45°$, where the phase jumps abruptly. It is important to note that under ideal conditions, the orientation of the nodal line is expected to be arbitrary, and the value it assumes in the simulation is a result of numerical residuals. As the flow velocity increases to $U_\infty = 55$ m/s, an incremental linear increase in the acoustic pressure phase over the cavity circumference indicates that the acoustic mode is spinning. The phase angle increases over the diametral coordinate $\theta$, as the peaks spin around the symmetry axis. Some deviation is evident as the behavior is not purely spinning. At the peak of the excitation of the spinning diametral mode, a nearly linear phase pattern is observed at $U_\infty = 64$ m/s. As all phases are referred to the phase of the monitor $p_1$ with a physical azimuthal location of $\theta = 0$, the phase angles $\phi$ and $\theta$ coincide with each other at all locations. With a further increase in the upstream flow velocity to $U_\infty = 66$ m/s, a partially spinning mode is observed, with deviations of the phase angles $\phi$ from the azimuthal location $\theta$ opposite to the deviations before the peak of resonance. At $U_\infty = 75$ m/s, no diametral mode is excited, and the pattern of the phase angle shows a steady phase of $\phi = 0$, indicating that all locations are in phase with each other. As expected, the longitudinal mode is not capable of showing any spinning characteristics due to its cylindrical symmetry.

## V. DYNAMICS OF THE FLOW–ACOUSTIC COUPLING

For the coupled flow–acoustic field during resonance excitation, strong oscillations exert a strong influence on the flow field. The periodic oscillations in the flow field, in turn, provide the adequate feedback to sustain the energy transfer from the flow to the acoustic field. As a result, the flow fields are expected to follow different patterns according to the pressure and acoustic particle velocity distributions of the excited acoustic modes. Due to the cylindrical


Published under license by AIP Publishing

symmetry of the cavity configuration, it is convenient to investigate the distribution of flow velocity over its cross section using the cylindrical coordinates $x$ in the streamwise direction, $R$ in the radial direction outward from the center, and $\theta$ counterclockwise and normal to the other two directions everywhere.

Figures 8 and 9 show the instantaneous distribution of the radial and tangential components of the flow velocity, respectively, over the cavity cross section at the middle of the distance between the leading and trailing edges. Four different instants over the acoustic cycle are shown for each upstream flow velocity, equivalent to the cases discussed in Fig. 6 (multimedia view). Figure 8 shows that the radial component of the flow velocity $u_R$ reaches up to ±0.25 of the upstream velocity for the three cases. This component oscillates over the acoustic cycle, resembling a significant oscillating momentum injection into and out of the cavity. The manner in which this injection occurs clearly influences how the acoustic mode materializes.

At $U_\infty$ = 50 m/s, at which a stationary diametral mode is excited, a corresponding stationary behavior is seen in Fig. 8(a) for the radial flow velocity component. The radial velocity reaches a maximum on one side of the antinodal plane and a minimum on the other side. The two sides then vary toward $u_R$ = 0 and then reverse their previous values. A full cycle is then completed as all radial velocities reach the value of $u_R$ = 0 for the second time.

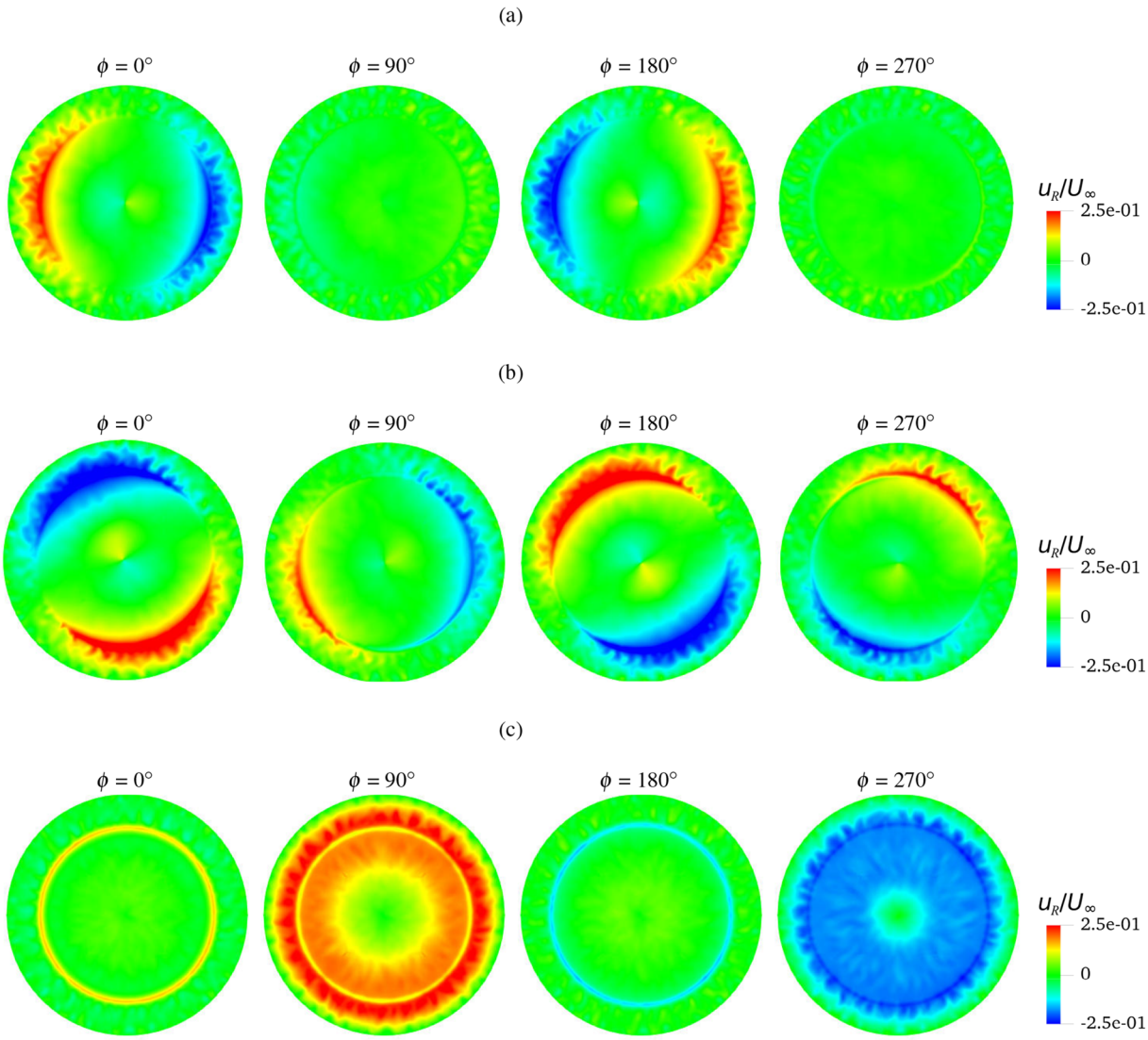



**FIG. 8**. The radial velocity component $u_R$ normalized by the upstream velocity in the middle cross section of the cavity at four equally spaced instants of the acoustic cycle at three different flow velocities. (a) Stationary acoustic diametral mode, $U_\infty$ = 50 m/s, (b) spinning acoustic diametral mode, $U_\infty$ = 64 m/s, and (c) longitudinal mode, $U_\infty$ = 75 m/s.


Published under license by AIP Publishing

The antisymmetric oscillating nature of the radial velocity means that momentum is injected in an oscillating manner so that at any instant, the flow moves toward one of two cavity sides. The two sides correspond to the two fixed outer antinodes seen in Fig. 6(a) (multimedia view). This oscillation drives the acoustic pressure to increase and decrease while the antinode is stationary. The tangential velocity component $u_\theta$ is shown in Fig. 9(a) for $U_\infty$ = 50 m/s. The center of the cavity cross section is a symmetry point for an oscillating pattern of the tangential flow velocity component. Locations with a counterclockwise flow direction fall to a tangential velocity of $u_\theta = 0$ and then reverse their directions and vice versa. The maximum and minimum values of $u_\theta$ occur on a line that coincides with the nodal pressure plane and indicate a momentum injection from one half of the cross section to the other. Most notably, this line is stationary during the excitation of the acoustic resonance at $U_\infty$ = 50 m/s.

The radial and tangential velocity components during the pure spinning diametral mode excitation at $U_\infty$ = 64 m/s, shown in Figs. 8(b) and 9(b), indicate a significantly different behavior. An antisymmetric pattern of the normalized radial velocity $u_R/U_\infty$ is visible at all instants. An important feature of this pattern is its rotation around the axis of the cavity. The location of the maximum and minimum values of the radial velocity component coincides with the leading and trailing edges, and therefore, this component indicates flow momentum injection into or out of the cavity from the main

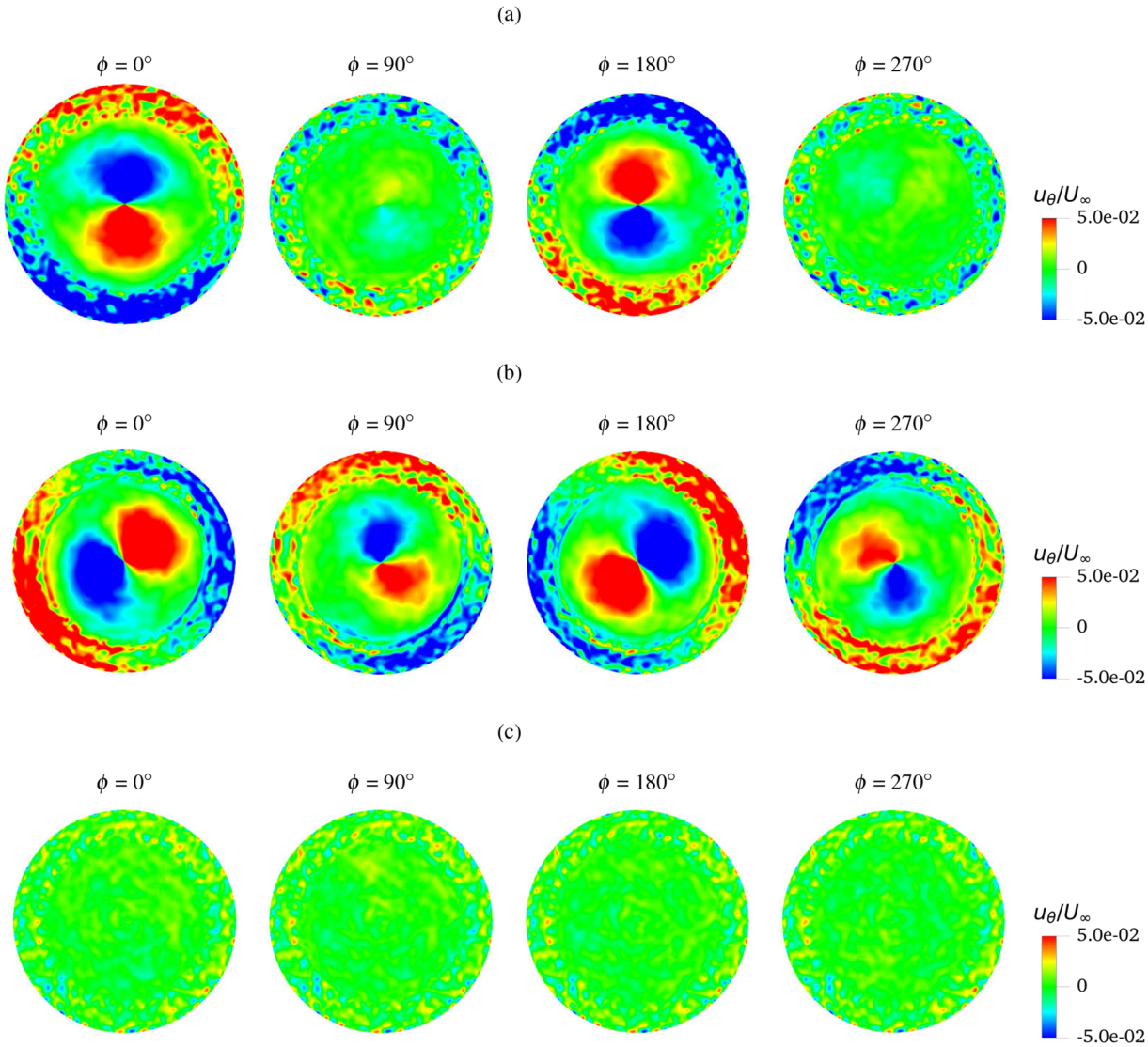



**FIG. 9**. The tangential velocity component $u_\theta$ normalized by the upstream velocity in the middle cross section of the cavity at four equally spaced instants of the acoustic cycle at three different flow velocities. (a) Stationary acoustic diametral mode, $U_\infty$ = 50 m/s, (b) spinning acoustic diametral mode, $U_\infty$ = 64 m/s, and (c) longitudinal mode, $U_\infty$ = 75 m/s.


Published under license by AIP Publishing

pipe. Moreover, Fig. 9(b) indicates an antisymmetric pattern of $u_\theta$ within the cavity region, where the flow rotates toward one side of the cavity and away from the other side, resulting in an increase and a decrease of acoustic pressure in these locations, respectively. The two locations stay opposite to each other while rotating along the cavity wall in one complete cycle. At the same time, in the inner circle $r \leq Dp/2$, the tangential velocity has opposite directions on the two sides of the circle. The two sides are separated by a line where $u\theta = 0$, which rotates at the same frequency as that of the acoustic spinning mode. The patterns of $u_R$ and $u_\theta$ observed during the excitation of the pure spinning diametral mode indicate that the flow momentum injection is continuous throughout the cycle, but its direction changes continuously so that it fuels an increase in the pressure at different locations of the cavity for each instant. Such a continuous change in the direction provides the necessary phasing for the pressure to peak in a rotating pattern so that the maximum pressure amplitude exists at some points at any instance of the cycle.

On the other hand, the patterns of the normalized radial and tangential velocity components shown in Figs. 8(c) and 9(c) for the longitudinal mode excitation are completely different. To drive a simultaneous increase in the acoustic pressure with the pattern shown in Fig. 6(c) (multimedia view), an oscillating flow cycle is required in the streamwise direction. The sudden change of area due to the presence of the cavity drives the oscillating flow periodically inward or outward as the pressure increases or decreases, respectively. The pattern of $u_R$ shows the initiation of this flow injection outward, then a dominant outward flow, which then ceases into an initiation of an inward flow at the cavity mouth circle, and then a dominantly inward flow. This cycle would give rise to a cycle of antisymmetric pressure increases and decreases at the wall and at the cavity center, which is clearly observed in Fig. 6(c) (multimedia view). Interestingly, Fig. 9(c) shows that no significant tangential momentum is present at any instant of the cycle. This results in no antisymmetric components across the cavity $R$–$\theta$ cross section. The acoustic pressure over the whole cross section is in-phase over the cycle, and therefore, no flow inertia is needed to drive the oscillating behavior in the tangential direction. Therefore, it can be concluded that the pattern of radial flow velocity component $u_R$ is responsible for maintaining the cylindrical acoustic pressure nodal plane, which coincides with the cavity mouth. It can also be observed that variations in $u_\theta$ are responsible for sustaining a linear acoustic pressure nodal plane that splits the cross section into two parts for the diametral modes, which is not observed for the longitudinal mode.

The defining feature of the flow dynamics associated with each of the three different excited acoustic modes are the dynamics of vortex separation and impingement. The resulting perturbations due to these dynamics and the feedback thereof are the main source of energy that drives the acoustic oscillations. During lock-in, the synchronization of these perturbations with the acoustic pressure oscillations initiates and then sustains the resonant conditions. It is, therefore, critical to understand how this process can adapt to the different patterns of acoustic and flow fields, such as those discussed above, to achieve resonance excitation.

Figure 10 shows iso-surfaces of the instantaneous $Q$ criterion during the excitation of acoustic resonance at three different flow velocities that drive three different azimuthal patterns of the acoustic pressure. To the left of Fig. 10, the iso-surfaces are superimposed on contours of instantaneous vorticity to identify the cores of the vortices on one streamwise plane for clarity. Definitive differences between the nature of the separating vortices, evident in Fig. 10, can be identified by examining the vortical structures as they separate at the leading edge, travel across the cavity mouth, and impinge on the trailing edge, as sketched in the right side of Fig. 10. At $U_\infty = 50$ m/s, during the excitation of a stationary acoustic mode with two antisymmetric spatial sides, a clear dislocation of vortices can be seen across the straight nodal pressure line. This nodal line is stationary and experiences no oscillations of acoustic pressure, which is explained for this case by the lack of separation and impingement over its length. Another notable feature for this mode is that the cavity is split by this streamwise nodal plane into two sides, seen in this figure to be the upper and lower halves. As mentioned before, this is an arbitrary location, despite being stationary in time. In each of the two halves, crescents of vortices, perfectly aligned in successive $R$–$\theta$ planes, separate alternately and lead to an antisymmetric impingement. This pattern results in alternating pressure oscillations that in turn drive the pressure to rise and fall antisymmetrically.

The vortical pattern during the excitation of the spinning diametral mode at $U_\infty = 64$ m/s has a different nature. In contrast to vortical crescents, a continuous helix of vortices connects the upstream and the downstream edges. Two complete revolutions of the helix are observed, signaling the second shear layer mode. Over time, the helix spins at a fixed pace so that the separation and impingement points rotate. At the peak of acoustic resonance, near $U_r = 0.93$, the frequency of vortex separation and impingement coincides with the acoustic mode frequency so that the acoustic pressure of this mode passes through a full cycle at the same time the helix makes a complete revolution and as the vortex passes between the leading and trailing edges. As a result, the separation and impingement points are connected by the shortest path possible over the cavity mouth, enhancing the feedback mechanism.

In contrast, the longitudinal mode excitation requires separation and impingement to occur uniformly and simultaneously along the whole leading and trailing edges, respectively. The vortical structures required to achieve this objective are vortical rings, continuous and aligned in successive $R$–$\theta$ planes. These rings also provide the same timing condition so that the path from the leading edge to the trailing edge is straight and as short as possible, explaining the increase in acoustic pressure as the longitudinal mode gets excited, as seen in Fig. 5.

To get a more detailed insight into the interaction of the acoustic and flow fields during acoustic resonance excitation, the polar plots in Fig. 11 (multimedia view) show the distribution of the acoustic pressure and shear layer vorticity $\omega = \sqrt{\omega_y^2 + \omega_z^2}$ over the cavity mouth. Values are shown near the separation point, at a distance of $0.1L$ from the leading edge, during excitation of acoustic resonance at $U_\infty = 50$ m/s. Four instants over the cycle are shown, corresponding to the same instants shown in Figs. 6–9. For this stationary mode, the profile of acoustic pressure clearly shows an oscillating behavior. The acoustic pressure keeps a circular profile, with its center oscillating back and forth in a straight line. At the same time, the profile of vorticity resembles a slightly distorted circle where deviation from the circular pattern occurs in one direction, parallel to the oscillating axis of the acoustic pressure. A phase angle is observed so that


Published under license by AIP Publishing

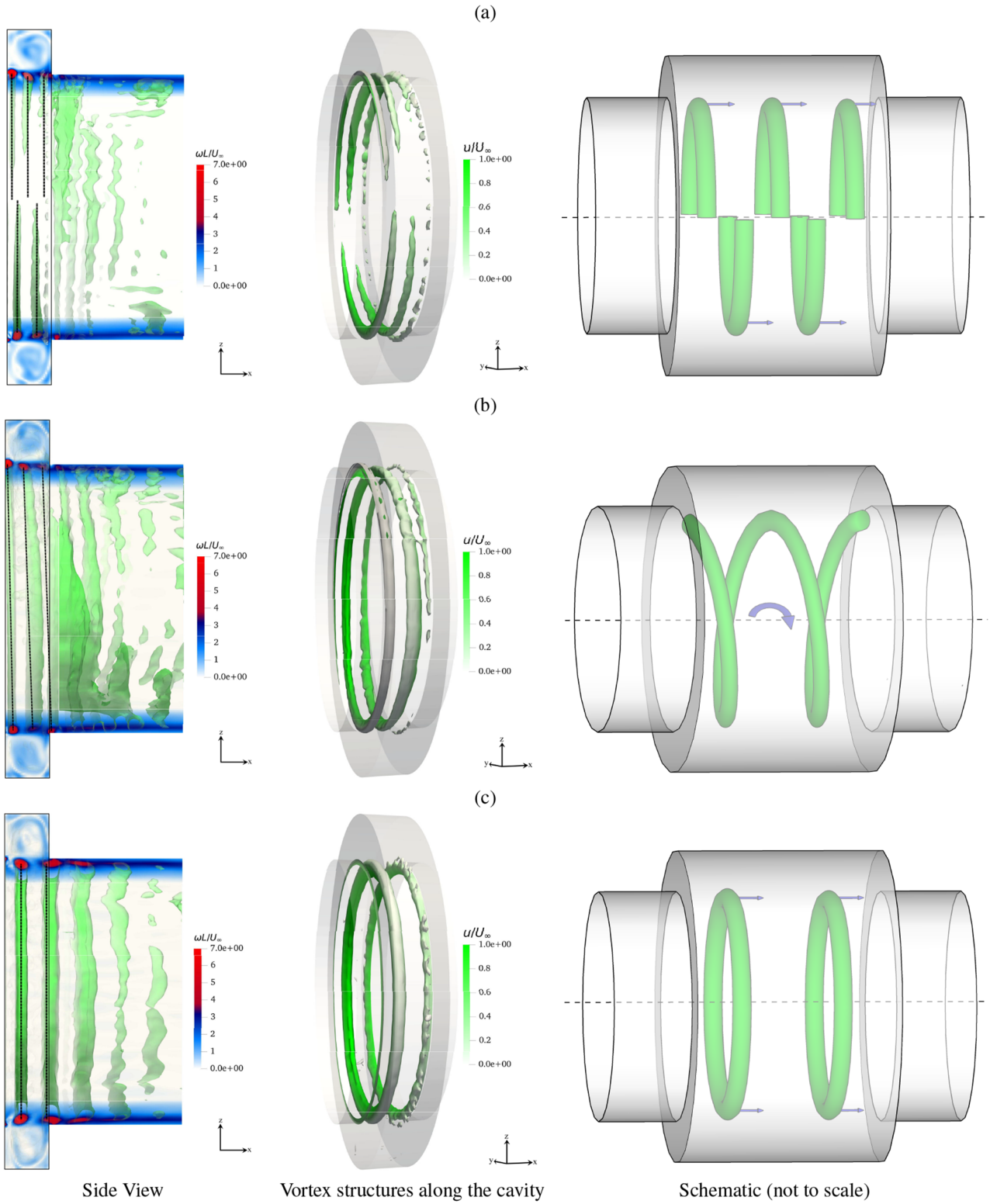



**FIG. 10**. The dynamics of the vortex separation and impingement for the axisymmetric cavity at three different flow velocities. Instantaneous iso-surfaces of the Q criterion at $Q = 10^6\ s^{-2}$ colored according to the flow velocity are imposed on two-dimensional contours of vorticity. (a) $U_\infty$ = 50 m/s, (b) $U_\infty$ = 64 m/s, and (c) $U_\infty$ = 75 m/s.


Published under license by AIP Publishing

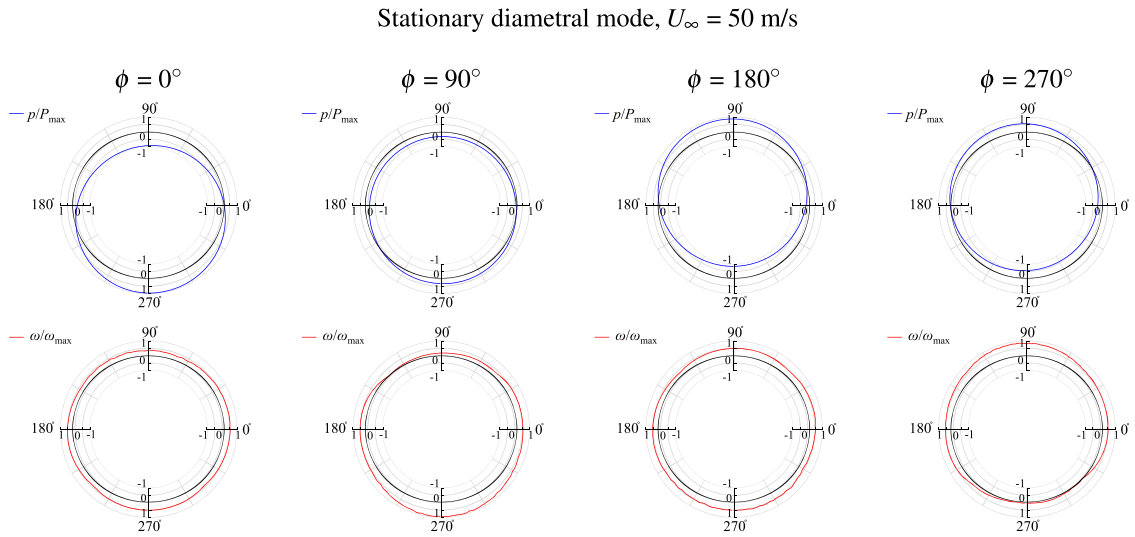



**FIG. 11**. The distribution of the acoustic pressure and the vorticity $\omega$ in the $y$–$z$ plane over the cavity mouth at a distance of 0.1 $L$ from the leading edge during excitation of acoustic resonance at $U_\infty$ = 50 m/s. Multimedia view: https://doi.org/10.1063/5.0026552.4

when the acoustic pressure is close to zero at all locations, at $\phi$ = 90, the vorticity has a peak value. As the pressure reaches opposite maximum and minimum values at $\phi$ = 180°, the vorticity falls again to zero at the same location. The fixed azimuthal location of the antinodes of acoustic pressure, coinciding with vorticity minima, clearly indicates that the oscillating nature of the two patterns is related to the stationary azimuthal behavior of this diametral mode.

In contrast, Fig. 12 (multimedia view) shows polar plots of acoustic pressure and vorticity during the excitation of the spinning diametral mode at $U_\infty$ = 64 m/s under the same conditions of Fig. 11 (multimedia view). The spinning behavior of the two modes can clearly be identified by analyzing the development of $p$ and $\omega$ at the four instants of the cycle. A circular pattern of the acoustic pressure keeps its shape, but spins around the center of the coordinate center with a constant eccentricity. Likewise, the vorticity profile takes the shape of a circle that resembles the separation of vortices at the leading edge. Note that the profile shown, at a distance of 0.1 $L$, is expected to be different at each cross section over the cavity length due to the rotation of the helix in Fig. 10(b). However, the overall profile shape should not change. As a result,

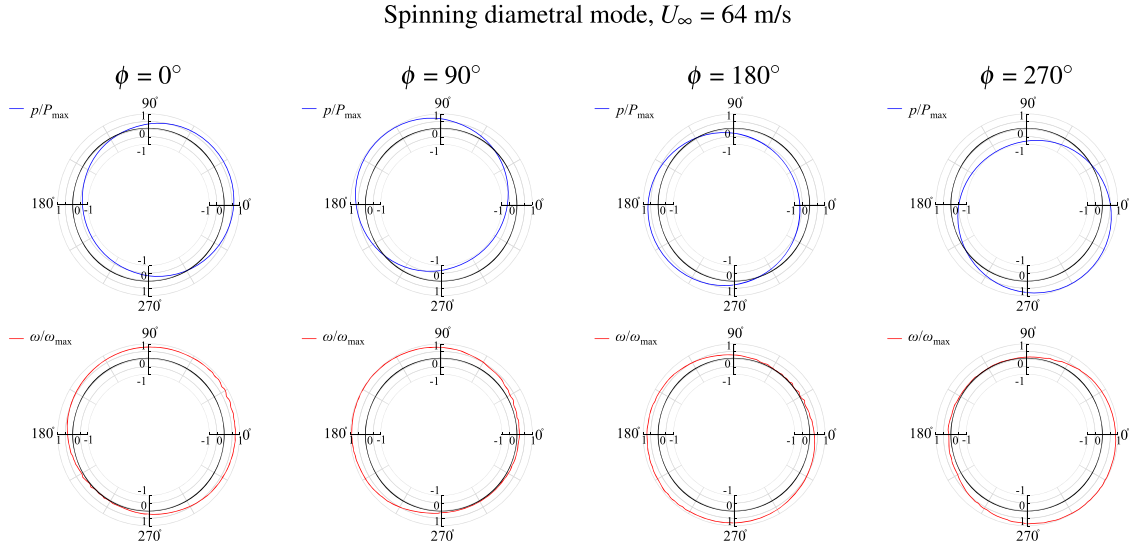



**FIG. 12**. The distribution of the acoustic pressure and vorticity $\omega$ over the cavity mouth at a distance of 0.1$L$ from the leading edge during excitation of acoustic resonance at $U_\infty$ = 64 m/s. Multimedia view: https://doi.org/10.1063/5.0026552.5


Published under license by AIP Publishing

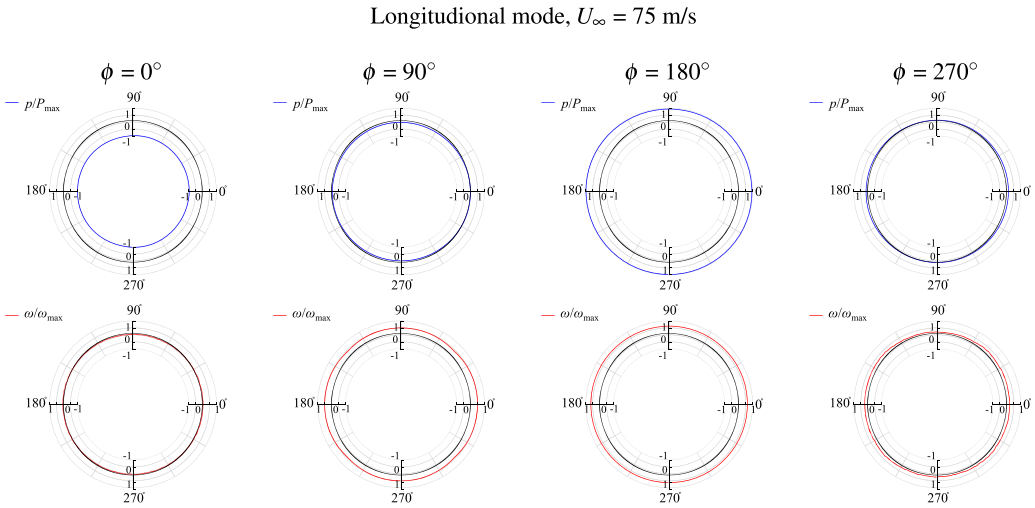



**FIG. 13**. The distribution of the acoustic pressure and vorticity over the cavity mouth at a distance of 0.1*L* from the leading edge during excitation of acoustic resonance at $U_\infty$ = 75 m/s. Multimedia view: https://doi.org/10.1063/5.0026552.6

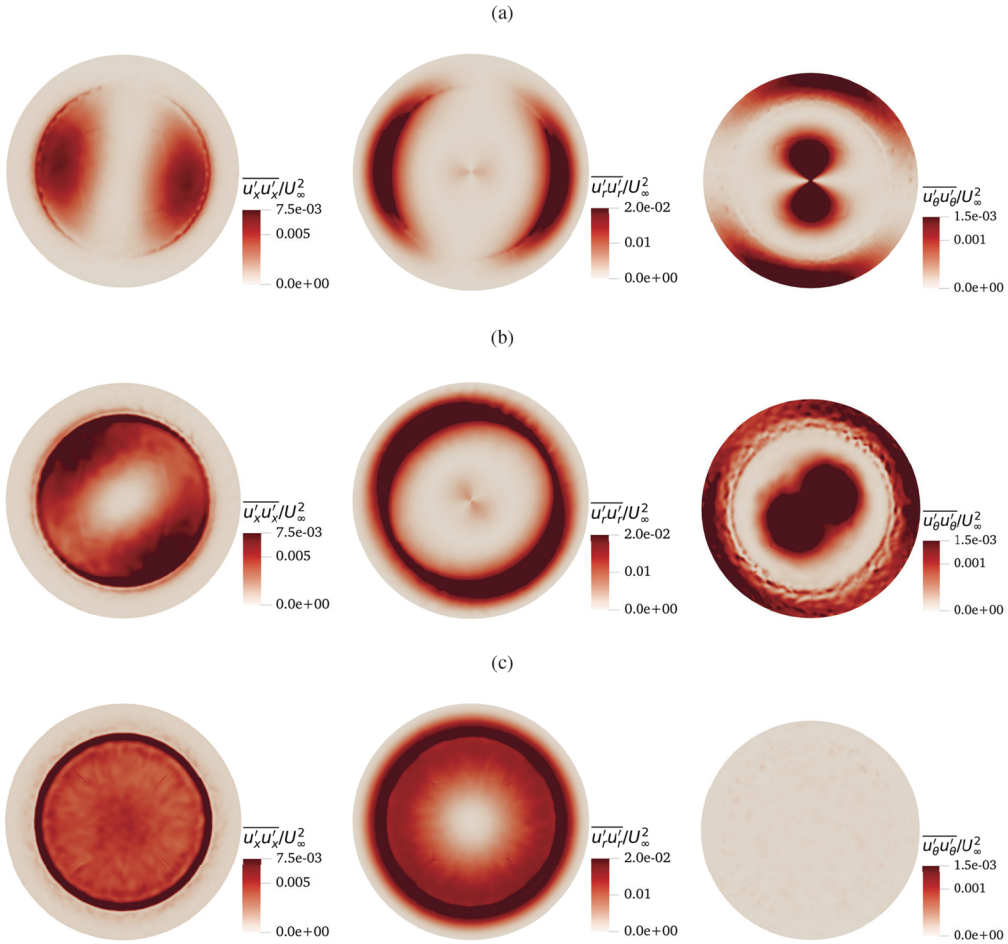



**FIG. 14**. Normal Reynolds stresses calculated using velocities in the cylindrical coordinates $u_x$, $u_R$, and $u_\theta$ during excitation of acoustic resonance at three different azimuthal mode behaviors. (a) Stationary acoustic diametral mode, $U_\infty$ = 50 m/s, (b) spinning acoustic diametral mode, $U_\infty$ = 64 m/s, and (c) longitudinal mode, $U_\infty$ = 75 m/s.


Published under license by AIP Publishing

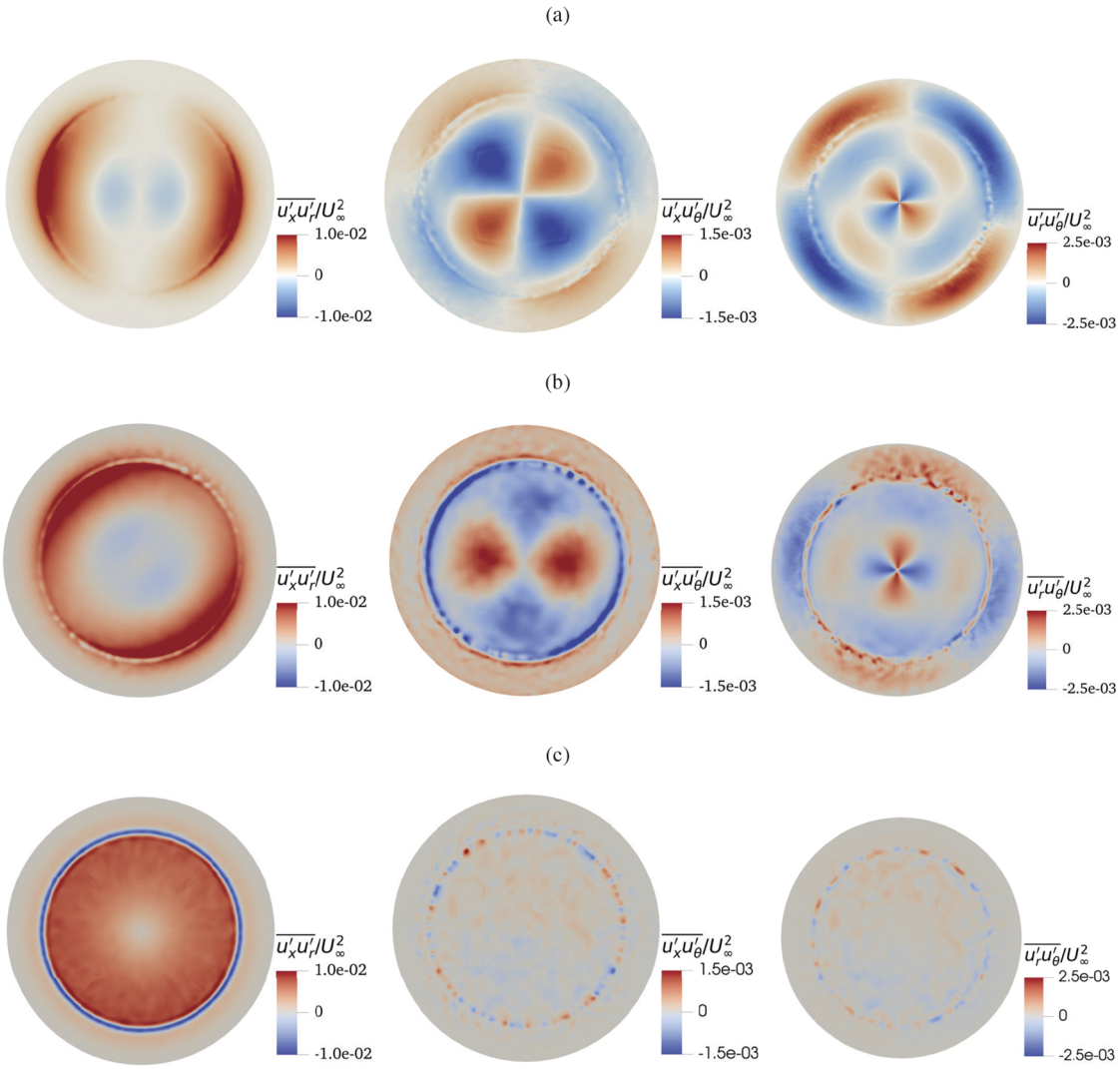



**FIG. 15**. Reynolds shear stresses calculated using velocities in the cylindrical coordinates $u_x$, $u_R$, and $u_\theta$ during excitation of acoustic resonance at three different azimuthal mode behaviors. (a) Stationary acoustic diametral mode, $U_\infty$ = 50 m/s, (b) spinning acoustic diametral mode, $U_\infty$ = 64 m/s, and (c) longitudinal mode, $U_\infty$ = 75 m/s.

the circular profile spins so that its maximum value, corresponding to a passing vortex, rotates and stays opposite to the location with $\omega = 0$, which corresponds to a gap between two successive vortices.

Figure 13 (multimedia view) presents a starkly different behavior of the acoustic pressure and vorticity during the excitation of the longitudinal mode at $U_\infty$ = 75 m/s. The pattern of the acoustic pressure pulsates outward and collapses inward in one complete cycle, driven by the flow momentum pouring into and then out of the cavity as discussed earlier. The vorticity profile is also circular at all instants as the vortex shedding process is synchronous along the whole leading edge. The vortices passing in the form of successive rings result in the pulsating behavior of the vorticity profile, which has a phase with the acoustic pressure pattern. The exact phase angle would vary according to the location of the cross section. This pattern leads to symmetric pulsations of pressure that can drive acoustic resonance in the longitudinal direction.

From the previous discussion, it is evident that the excitation of acoustic resonance is initiated and sustained by the fluctuating flow components in the shear layer. To identify the distribution of these fluctuations, which resembles potential acoustic sources, the turbulent Reynolds stresses are discussed. The distribution of the normal Reynolds stresses $\overline{u'_x u'_x}$, $\overline{u'_R u'_R}$, and $\overline{u'_\theta u'_\theta}$ is shown in Fig. 14 during the excitation of the three different acoustic resonant modes. The stresses are shown for the cross section of the cavity at $0.5L$ from the leading and trailing edges. At $U_\infty$ = 50 m/s, fluctuations seen in Fig. 14(a) for the $x$ and $R$ normal stresses are dominant over two opposite halves of the cavity mouth. The crescent-shaped


Published under license by AIP Publishing

distribution points to potential excitation of the acoustic mode that results in the formation of the cylindrical nodal plane between the two halves of the cavity. Fluctuations in the $\theta$ normal stress are stronger in the region closer to the axis of the cavity, which indicates that they are related to the oscillating flow that builds up antisymmetric pressure across the straight nodal pressure plane. A different pattern is shown in Fig. 14(b), where the excitation of the spinning acoustic mode results in stronger fluctuations. Unlike the pattern split in half by the nodal line, the rotating nodal line results in fluctuations at all locations over the course of the acoustic cycle, and therefore, the $x$ and $R$ normal stresses are axisymmetric around the cavity center point. The longitudinal mode excitation corresponds to a different pattern of fluctuations shown in Fig. 14(c). Strongest fluctuations occur in the $x$ normal stresses, as they drive a longitudinal mode with strong pressure variations in the streamwise direction. Oscillations are concentrated around the cavity mouth. This pattern is associated with a fairly equal distribution of fluctuations in the $R$ direction, as a momentum flux passes uniformly into and out of the cavity. No significant fluctuations occur in the tangential direction as suggested by the absence of any normal $\theta$ stress everywhere.

Shear Reynolds stresses are shown in Fig. 15 and suggest critical differences in the interaction of the flow velocity fluctuations leading to the different azimuthal behaviors in the three cases, asserting the discussion above. While the nodal plane is visible in the patterns of $\overline{u'_x u'_R}$, $\overline{u'_x u'_\theta}$, and $\overline{u'_R u'_\theta}$ during the excitation of the stationary mode, it can be seen that the $\overline{u'_x u'_R}$ stress is significantly stronger around the cavity mouth than the other two shear stresses suggesting that fluctuations in the tangential $\theta$ direction are insignificant, affirming the lack of rotation. On the other hand, the cavity mouth nodal plane has significantly higher components of $\overline{u'_x u'_\theta}$ at $U_\infty$, where a rotating mode is excited. Favourable interaction of the streamwise and tangential fluctuations is critical to initiate and sustain the spinning flow dynamics that corresponds to the helix vortex structure. Finally, the longitudinal mode has significant shear stresses only due to the interaction of the $x$ and $R$ directions. Such fluctuations would only be able to excite longitudinal waves and can initiate neither a spinning dynamic nor an antisymmetric pressure pattern, due to the lack of any significant shear stress with a tangential $\theta$ component.

## VI. CONCLUSION

In this work, a large eddy simulation is used to solve the compressible Navier–Stokes equations in order to investigate the dynamics of the coupled flow–sound field during excitation of acoustic resonance by the flow over an axisymmetric cavity with an aspect ratio of $L/d = 1$. A one-equation subgrid-scale kinetic energy LES turbulence model was used to simulate the acoustic resonance excitation mechanism over a range of flow velocities that lead to the excitation of three different acoustic modes with different acoustic pressure patterns and flow dynamics. The model predicts well the excitation of acoustic resonance and development of the acoustic pressure and shows a good agreement with available experimental observations. It was found that, at low flow velocities, a stationary diametral acoustic mode is excited, with stationary nodal planes. During the excitation of this mode, the acoustic pressure reciprocates locally on both sides of the nodal planes. A further increase in the flow velocity resulted in the excitation of a spinning diametral acoustic mode. In this case, a spinning nodal plane rotates around the streamwise axis of the pipe. A further increase in the flow velocity resulted in the excitation of a longitudinal acoustic mode, characterized by the existence of a cylindrical nodal plane concentric with the cavity leading and trailing edges. In order to understand the nature of the aeroacoustic coupling during the excitation of the different acoustic modes, the flow dynamics for each case is investigated. During the excitation of the stationary diametral mode, the flow field in the middle cross section of the cavity illustrates that the radial and tangential velocities were following a reciprocating behavior around the acoustic pressure nodal and antinodal lines. Iso-surfaces of the instantaneous Q criterion demonstrated the existence of two antisymmetric series of vortical crescents that are disconnected at those pressure nodal lines. The alternating separation of these vortex tubes drives the pressure to rise and fall in an antisymmetric pattern. The flow field during the excitation of spinning diametral mode excitation shows that the radial and tangential velocities followed a spinning pattern along the cross section of the cavity while keeping their antisymmetric distribution during the acoustic cycle. Moreover, the spinning mode excitation was accompanied by a continuous helix of vortices that connects the upstream and the downstream edges, forming the shortest path possible over the cavity mouth, which enhanced the feedback mechanism. On the other side, in case of excitation of longitudinal mode, the radial velocity showed a pulsating behavior that complemented the acoustic pressure cycle. In this case, the flow field had no significant velocity or Reynolds stresses in the circumferential direction. The separation of the vortex took place in a uniform manner along the separation edge, leading to the formation of complete rings of vortex tubes that impinge on the downstream edge leading to an increase in the values of the acoustic pressure.

## ACKNOWLEDGMENTS

The authors would like to acknowledge the financial support provided by the Natural Sciences and Engineering Research Council of Canada (NSERC).

## DATA AVAILABILITY

The data that support the findings of this study are available from the corresponding author upon reasonable request.

## REFERENCES

[1] S. Ziada *et al.*, "An in-depth study of vortex shedding, acoustic resonance and turbulent forces in normal triangle tube arrays," J. Fluids Struct. **12**, 717–758 (1998).

[2] A. Mohany, "Self-excited acoustic resonance of isolated cylinders in cross-flow," Nucl. Rev. **1**, 45–55 (2014).

[3] M. Shaaban and A. Mohany, "Phase-resolved PIV measurements of flow over three unevenly spaced cylinders and its coupling with acoustic resonance," Exp. Fluids **60**, 71 (2019).

[4] M. R. Islam, M. Shaaban, and A. Mohany, "Vortex dynamics and acoustic sources in the wake of finned cylinders during resonance excitation," Phys. Fluids **32**, 075117 (2020).

[5] M. R. Islam and A. Mohany, "Vortex shedding characteristics in the wake of circular finned cylinders," Phys. Fluids **32**, 045113 (2020).


Published under license by AIP Publishing

[6]O. Afifi and A. Mohany, "Parametric investigation of the flow-sound interaction mechanism for single cylinders in cross-flow," J. Pressure Vessel Technol. **142**(2), 021404 (2020).
[7]H. Al-Muslim, N. Al-Nasri, and M. Al-Hashem, "The danger of piping failure due to acoustic-induced fatigue in infrequent operations: Two case studies," J. Pressure Vessel Technol. **135**(6), 064501 (2013).
[8]T. Lato and A. Mohany, "Passive damping of pressure pulsations in pipelines using Herschel-Quincke tubes," J. Sound Vib. **448**, 160–177 (2019).
[9]K. Sachedina, A. Mohany, and M. Hassan, "Experimental study on damping acoustic pressure pulsations in pipeline systems using Helmholtz resonators," J. Pressure Vessel Technol. **142**, 021403 (2020).
[10]P. Wang, Y. Deng, and Y. Liu, "Vortex dynamics during acoustic-mode transition in channel branches," Phys. Fluids **31**, 085109 (2019).
[11]Y. Uchiyama and R. Morita, "Combined effects of steam wetness and pressure on characteristics of acoustic resonance amplitude in closed side branch," J. Pressure Vessel Technol. **143**(1), 011402 (2020).
[12]J. R. Dawson and N. A. Worth, "Flame dynamics and unsteady heat release rate of self-excited azimuthal modes in an annular combustor," Combust. Flame **161**, 2565–2578 (2014).
[13]S. S. Rashwan, A. Mohany, and I. Dincer, "Investigation of self-induced thermoacoustic instabilities in gas turbine combustors," Energy **190**, 116362 (2020).
[14]B. A. W. Smith and B. V. Luloff, "The effect of seat geometry on gate valve noise," J. Pressure Vessel Technol. **122**, 401–407 (2000).
[15]S. Ziada, A. Oengören, and A. Vogel, "Acoustic resonance in the inlet scroll of a turbo-compressor," J. Fluids Struct. **16**, 361–373 (2002).
[16]R. Parker and D. C. Pryce, "Wake excited resonances in an annular cascade: An experimental investigation," J. Sound Vib. **37**, 247 (1974).
[17]S. Ziada and P. Lafon, "Flow-excited acoustic resonance: Excitation mechanism, design guidelines and counter measures," Appl. Mech. Rev. **66**(1), 010802 (2014).
[18]M. Mazur, H. T. Nygård, J. R. Dawson, and N. A. Worth, "Characteristics of self-excited spinning azimuthal modes in an annular combustor with turbulent premixed bluff-body flames," Proc. Combust. Inst. **37**, 5129–5136 (2019).
[19]C. Carmicino, "Acoustics, vortex shedding, and low-frequency dynamics interaction in an unstable hybrid rocket," J. Propul. Power **25**, 1322–1335 (2009).
[20]S. Hein and W. Koch, "Acoustic resonances and trapped modes in pipes and tunnels," J. Fluid Mech. **605**, 401–428 (2008).
[21]K. Aly and S. Ziada, "Review of flow-excited resonance of acoustic trapped modes in ducted shallow cavities," J. Pressure Vessel Technol. **138**(4), 040803 (2016).
[22]J. Xu, J. Lei, J. Wu, and K. Zhang, "The three-dimensional characteristics of the unsteady wall-pressure in a low-Mach-number rectangular cavity flow with Rossiter model oscillation," Exp. Fluids **58**, 109 (2017).
[23]D. Rockwell and E. Naudascher, "Review-self-sustaining oscillations of flow past cavities," J. Fluids Eng. **100**, 152–165 (1978).
[24]J. Rossiter, "Wind tunnel experiments on the flow over rectangular cavities at subsonic and transonic speeds," RAE Technical Report No. 64037, 1964.
[25]S. Ziada, H. Ng, and C. E. Blake, "Flow excited resonance of a confined shallow cavity in low Mach number flow and its control," J. Fluids Struct. **18**(1), 79–92 (2003).
[26]P. Wang and Y. Liu, "Intensified flow dynamics by second-order acoustic standing-wave mode: Vortex-excited acoustic resonances in channel branches," Phys. Fluids **31**, 035105 (2019).
[27]A. Omer, A. Mohany, and M. Hassan, "Effect of impingement edge geometry on the acoustic resonance excitation and Strouhal numbers in a ducted shallow cavity," Wind Struct. **23**, 91–107 (2016).
[28]S. Mohamed, H. Graf, and S. Ziada, "Measurement of the excitation source of an axisymmetric shallow cavity shear layer," J. Pressure Vessel Technol. **140**(3), 031304 (2018).
[29]J. Golliard, S. Belfroid, O. Vijlbrief, and K. Lunde, "Direct measurements of acoustic damping and sound amplification in corrugated pipes with flow," in *ASME 2015 Pressure Vessels and Piping Conference* (American Society of Mechanical Engineers, 2015), Vol. 56970, p. V004T04A037.
[30]A. A. Shaaban and S. Ziada, "Fully developed building unit cavity source for long multiple shallow cavity configurations," Phys. Fluids **30**, 086105 (2018).
[31]M. Shaaban and A. Mohany, "Passive control of flow-excited acoustic resonance in rectangular cavities using upstream mounted blocks," Exp. Fluids **56**, 72 (2015).
[32]K. M. Nair and S. Sarkar, "Large eddy simulation of self-sustained cavity oscillation for subsonic and supersonic flows," J. Fluids Eng. **139**(1), 011102 (2017).
[33]D. V. Evans, M. Levitin, and D. Vassiliev, "Existence theorems for trapped modes," J. Fluid Mech. **261**, 21–31 (1994).
[34]S. Hein, W. Koch, and L. Nannen, "Trapped modes and Fano resonances in two-dimensional acoustical duct-cavity systems," J. Fluid Mech. **692**, 257 (2012).
[35]J. J. Keller and M. P. Escudier, "Flow-excited resonances in covered cavities," J. Sound Vib. **86**(2), 199–226 (1983).
[36]K. Awny and S. Ziada, "Flow excitation of diametral acoustic modes of axisymmetric cavities," in *ASME 2006 Pressure Vessels and Piping/ICPVT-11 Conference* (American Society of Mechanical Engineers Digital Collection, 2006), pp. 115–123.
[37]K. Aly and S. Ziada, "Effect of mean flow on the trapped modes of internal cavities," J. Fluids Struct. **33**, 70–84 (2012).
[38]K. Aly and S. Ziada, "Flow-excited resonance of trapped modes of ducted shallow cavities," J. Fluids Struct. **26**(1), 92–120 (2010).
[39]K. Aly and S. Ziada, "Azimuthal behaviour of flow-excited diametral modes of internal shallow cavities," J. Sound Vib. **330**, 3666–3683 (2011).
[40]P. Oshkai and O. Barannyk, "Experimental investigation of flow-acoustic coupling in a deep axisymmetric cavity," in *ASME 2013 Pressure Vessels and Piping Conference* (American Society of Mechanical Engineers Digital Collection, 2013).
[41]M. Thirumoorthy, S. R. Chakravarthy, and P. V. G. Brahmanandam, "Shape effects of single axisymmetric cavity in a circular duct on flow induced acoustic oscillations," Aero. Sci. Technol. **67**, 181–192 (2017).
[42]P. Oshkai and O. Barannyk, "Quantitative visualization of unstable, acoustically coupled shear layers in deep axisymmetric cavities," in *ASME 2014 Pressure Vessels and Piping Conference* (American Society of Mechanical Engineers, 2014), Vol. 46018, p. V004T04A024.
[43]S. Ziada, M. Bolduc, and P. Lafon, "Flow-excited resonance of diametral acoustic modes in ducted rectangular cavities," AIAA J. **55**, 3817–3830 (2017).
[44]P. Wang and Y. Liu, "Influence of diametral acoustic mode on cavity flow dynamics: Zonal large eddy simulation and proper orthogonal decomposition," Phys. Fluids **32**, 075103 (2020).
[45]P. Wang and Y. Liu, "Spinning behavior of flow-acoustic resonant fields inside a cavity: Vortex-shedding modes and diametral acoustic modes," Phys. Fluids **32**, 085109 (2020).
[46]A. A. Shaaban and S. Ziada, "Effect of the separation distance on the aeroacoustic source of multiple shallow cavities," J. Fluids Eng. **141**(1), 011102 (2019).
[47]S. Benhamadouche, M. Arenas, and W. J. Malouf, "Wall-resolved large eddy simulation of a flow through a square-edged orifice in a round pipe at Re = 25,000," Nucl. Eng. Des. **312**, 128–136 (2017).
[48]C. Habchi, S. Russeil, D. Bougeard, J.-L. Harion, T. Lemenand, A. Ghanem, D. D. Valle, and H. Peerhossaini, "Partitioned solver for strongly coupled fluid-structure interaction," Comput. Fluids **71**, 306–319 (2013).
[49]C. Y. Lee and S. Cant, "Assessment of les subgrid-scale models and investigation of hydrodynamic behaviour for an axisymmetrical bluff body flow," Flow, Turbul. Combust. **98**, 155–176 (2017).
[50]A. Yoshizawa and K. Horiuti, "A statistically-derived subgrid-scale kinetic energy model for the large-eddy simulation of turbulent flows," J. Phys. Soc. Jpn. **54**, 2834–2839 (1985).
[51]A. K. Shukla and A. Dewan, "Openfoam based les of slot jet impingement heat transfer at low nozzle to plate spacing using four SGS models," Heat Mass Transfer **55**, 911–931 (2019).
[52]I. Marusic, J. P. Monty, M. Hultmark, and A. J. Smits, "On the logarithmic region in wall turbulence," J. Fluid Mech. **716**, 1 (2013).
[53]U. Piomelli, "Wall-layer models for large-eddy simulations," Prog. Aeronaut. Sci. **44**, 437–446 (2008).
[54]R. Pain, P.-E. Weiss, S. Deck, and J.-C. Robinet, "Large scale dynamics of a high Reynolds number axisymmetric separating/reattaching flow," Phys. Fluids **31**, 125119 (2019).
[55]M. Shaaban and A. Mohany, "Characteristics of acoustic resonance excitation by flow around inline cylinders," J. Pressure Vessel Technol. **141**(5), 051301 (2019).


Published under license by AIP Publishing